Dipole strength of ^{181}Ta for the evaluation of the ^{180}Ta stellar neutron capture rate

A. Makinaga,[1] R. Massarczyk,[2,3] R. Schwengner,[2] M. Beard,[4] F. Dönau,[2] M. Anders,[2,3] D. Bemmerer,[2] R. Beyer,[2] R. Hannaske,[2,3] A. R. Junghans,[2] M. Kempe,[2,3] T. Kögler,[2,3] M. Röder,[2,3] K. Schmidt,[2,3] and A. Wagner[2]

[1]*Meme Media Laboratory, Hokkaido University, North-10, West-8, North, Sapporo 060-0810, Japan*

[2]*Institute of Radiation Physics, Helmholtz-Zentrum Dresden-Rossendorf, 01328 Dresden, Germany*

[3]*Technische Universität Dresden, 01062 Dresden, Germany*

[4]*Department of Physics, University of Notre Dame, Notre Dame, Indiana 46556, USA*

(Received 12 January 2014; revised manuscript received 17 July 2014; published 2 October 2014)

The photoabsorption cross section of ^{181}Ta up to the neutron-separation energy is deduced using bremsstrahlung produced with an electron beam of 9.6 MeV energy. The analysis of the measured γ-ray spectra includes the quasicontinuum of levels at high energy. Simulations of γ-ray cascades are performed to estimate intensities of inelastic transitions and branching ratios of the ground-state transitions. The resulting photoabsorption cross section shows enhanced dipole strength in the energy range from 5 to 8 MeV, which may be related to a pygmy dipole resonance. The results of the present experiment are compared with predictions of a quasiparticle-random-phase approximation in a deformed basis. A combination of the present experimental data and (γ,n) data is used as an input to the statistical code TALYS applied to calculate cross sections and reaction rates of photonuclear reactions that are important for the nucleosynthesis of ^{180}Ta.

DOI: 10.1103/PhysRevC.90.044301 PACS number(s): 21.10.Pc, 24.60.Dr, 25.20.Dc, 27.70.+q

I. INTRODUCTION

The understanding of the γ-ray strength function (GSF) is one of the key challenges to solving nucleosynthetic puzzles. In the hot astrophysical plasma, nuclei are thermally populated between the ground and excited states. The stellar reaction rate within the statistical model, which is the sum of the photodisintegration rates from all states, weighted with the Boltzmann factor, requires not only the relevant nuclear level densities (NLDs), but also the transmission coefficients of photons and particles pertinent to the reaction [1]. It is known that the transmission coefficient for $E1$ γ rays from excited nuclei is directly related to the $E1$ GSF. Therefore, experimental cross sections for both the photoneutron reactions above the neutron-separation energy S_n and the photon-scattering reactions below S_n are important quantities for determining the GSF precisely. In addition, the GSF provides a significant contribution to information about neutron capture reactions that cannot be measured directly in the laboratory [2,3]. In such cases, the study of the inverse reaction is valuable. Neutron capture reactions are also of great interest to novel nuclear technologies such as nuclear transmutation using accelerator-driven systems.

The origin of ^{180m}Ta, which is the rarest nuclide in the solar system, has been widely discussed over the past 40 years [4–14]. Difficulties in understanding the creation of ^{180m}Ta arise from the various possible elemental production mechanisms, such as the slow (s) or rapid (r) neutron capture processes as well as the γ and ν processes.

Under the γ-process conditions in type-Ia supernovae, which correspond to a typical temperature of $T = (2$ to $3) \times 10^9$ K, ^{181}Ta produces ^{180m}Ta by emitting a neutron. Photodisintegration cross sections for ^{181}Ta were measured by using quasimonochromatic γ-ray beams from laser-Compton scattering at the National Institute of Advanced Industrial Science and Technology (AIST) in Japan. Whereas these experimental data for ^{181}Ta$(\gamma,n)^{180}$Ta and ^{181}Ta$(\gamma,n)^{180m}$Ta constrained the production rate of ^{180m}Ta, the uncertainty of the photodisintegration rate from below the neutron-separation energy still remains [9,10].

Alternatively, attempts have been made to explain ^{180m}Ta production in core-collapse supernovae via the neutral current (NC) reaction ^{181}Ta$(\nu,\nu'n)$ [15,16]. Such predictions show an overproduction of about 15% [17]. In theoretical investigations the results for the NC reaction are estimated to be about 4 to 5 times smaller than the result for the charged-current (CC) reaction ^{180}Hf$(\nu_e,e^-)^{180m}$Ta; however, the overproduction of ^{180m}Ta still remains [18].

The s-process contribution to ^{180}Ta has been studied by many authors [5–7,11–14]. The s-process includes branches into neutron capture as well as into β decay. The branching takes place at radiative nuclei with β-decay rates comparable to the neutron capture rate. Efforts to analyze s-process branching have been made to investigate stellar conditions such as neutron density and temperature [7,19].

A challenging attempt to measure the neutron capture reaction ^{180m}Ta$(n,\gamma)^{181}$Ta was made over the energy range 10–100 keV [5]. However, the data still have experimental uncertainties ranging from 8% to 67%, whereas the theoretical results overestimate the neutron capture cross section relative to experimental data. Thus, it is beneficial to estimate the neutron capture cross section by using statistical reaction codes with realistic input strength functions obtained from nuclear resonance fluorescence (NRF), ^{181}Ta(γ,γ'), and from the ^{181}Ta$(\gamma,n)^{180}$Ta reaction.

The deformed nuclide ^{181}Ta is also of special importance for the understanding of the nuclear many-body system. Dipole excitations at energies between 1.8 and 4 MeV were investigated in experiments at the former Stuttgart Dynamitron [20]. The dipole-strength distribution for energies up to S_n is of particular interest because enhanced strength on the low-energy tail of the giant dipole resonance (GDR), often

denoted as the "pygmy dipole resonance" (PDR) was found to be especially pronounced in ^{76}Se [21], ^{78}Se [22], nuclides with $Z = 42$ [23,24], $N = 50$ [25–28], around $N = 82$ [29–36], in ^{196}Pt [37], and in the doubly magic ^{208}Pb [38–40].

These circumstances motivated new measurements of photoabsorption cross sections of ^{181}Ta below the neutron-separation energy, which we present in the following. In Sec. II we describe the experimental procedure and the data analysis. In Sec. III the experimental results are compared with results of calculations on the basis of a quasiparticle random-phase approximation (QRPA). In Sec. IV we compare reaction rates calculated with the statistical code TALYS [41] using the present data as an input strength function, against results obtained using standard analytical strength functions.

II. EXPERIMENTAL PROCEDURES

A. Photon-scattering experiment

The NRF experiment on ^{181}Ta was performed using the bremsstrahlung facility γELBE [42] at the superconducting electron accelerator of the Helmholtz-Zentrum Dresden-Rossendorf (HZDR). Bremsstrahlung was produced by hitting a 7 μm niobium radiator with an electron beam of 9.6 MeV kinetic energy and an average current of 640 μA. The electron energy was chosen such that the flux is sufficiently high up to the neutron-separation energy $S_n = 7.6$ MeV. The bremsstrahlung was collimated by an Al collimator of a length of 2.6 m and an opening angle of 5 mrad starting with an entrance of 8 mm diameter. A cylindrical Al absorber of 10 cm length was placed between the radiator and the collimator entrance to reduce the intensity of the low-energy bremsstrahlung. The collimated photon beam impinged onto the target with a flux of several 10^8 MeV^{-1}s^{-1} in a spot of 38 mm diameter. The target was made of 2166.6 mg of natural Ta. It was combined with 200.0 mg of boron enriched to 99.5% in ^{11}B for the determination of the photon flux. Both materials were formed to disks of 20 mm diameter to enable an irradiation with a constant flux density over the target area.

The scattered photons were measured with four high-purity germanium (HPGe) detectors of 100% efficiency at 1.3 MeV relative to a NaI detector of 7.6 cm in length and 7.6 cm in diameter. All HPGe detectors were surrounded by escape-suppression shields made of bismuth germanate scintillation detectors. Two HPGe detectors were placed vertically at 90° relative to the photon-beam direction at a distance of 28 cm from the target. The other two HPGe detectors were placed horizontally at 127° to the beam at a distance of 32 cm from the target. To reduce the intensities of scattered low-energy photons, absorbers of 8 mm Pb plus 3 mm Cu were placed in front of the detectors at 90°, and 3 mm Pb plus 3 mm Cu were used for the detectors at 127°. Spectra of scattered photons were measured for 90 h. Part of a spectrum including events measured with the two detectors at 127° relative to the beam is shown in Fig. 1.

B. Photon-scattering method

In photon-scattering experiments the energy-integrated scattering cross section I_s of an excited state at the energy E_x

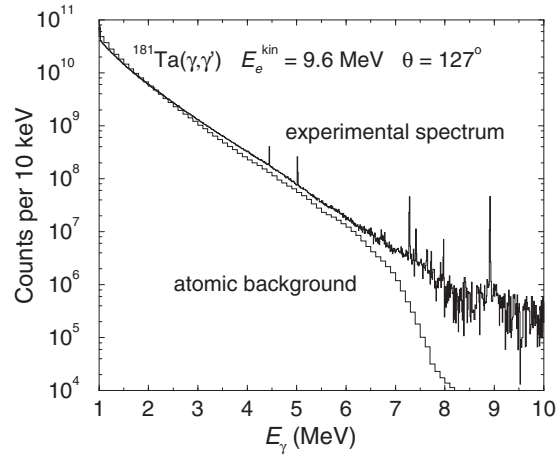

FIG. 1. Spectrum of photons scattered from ^{181}Ta, corrected for room background and detector response, and simulated spectrum of the atomic background, multiplied with efficiency and measuring time. The four most intense peaks belong to transitions in ^{11}B.

can be deduced from the measured intensity of the respective transition to the ground state (elastic scattering). It can be determined relative to the known integrated scattering cross sections $I_s(E_x^{\mathrm{B}})$ of states in ^{11}B [43,44]:

$$\frac{I_s(E_x)}{I_s(E_x^{\mathrm{B}})} = \left(\frac{I_\gamma(E_\gamma,\theta)}{W(E_\gamma,\theta)\Phi_\gamma(E_x)N_N}\right) \times \left(\frac{I_\gamma\left(E_\gamma^{\mathrm{B}},\theta\right)}{W\left(E_\gamma^{\mathrm{B}},\theta\right)\Phi_\gamma\left(E_x^{\mathrm{B}}\right)N_N^{\mathrm{B}}}\right)^{-1}. \quad (1)$$

Here, $I_\gamma(E_\gamma,\theta)$ and $I_\gamma(E_\gamma^{\mathrm{B}},\theta)$ denote the measured intensities of a considered ground-state transition at E_γ and of a ground-state transition in ^{11}B at E_γ^{B}, respectively, observed at an angle θ to the beam. $W(E_\gamma,\theta)$ and $W(E_\gamma^{\mathrm{B}},\theta)$ describe the angular correlations of these transitions. The quantities N_N and N_N^{B} are the numbers of nuclei in the ^{181}Ta and ^{11}B targets, respectively. The quantities $\Phi_\gamma(E_x)$ and $\Phi_\gamma(E_x^{\mathrm{B}})$ stand for the photon fluxes at the energy of the considered level and at the energy of a level in ^{11}B, respectively.

The integrated scattering cross section is related to the partial width of the ground-state transition Γ_0 according to

$$I_s = \int \sigma_{\gamma\gamma}\, dE = \left(\frac{\pi\hbar c}{E_x}\right)\frac{2J_x+1}{2J_0+1}\frac{\Gamma_0^2}{\Gamma}, \quad (2)$$

where $\sigma_{\gamma\gamma}$ is the elastic scattering cross section, E_x, J_x, and Γ denote energy, spin, and total width of the excited level, respectively, and J_0 is the spin of the ground state.

For the determination of the level widths, one is faced with two problems. First, a considered level can be fed by transitions from higher-lying states. The measured intensity of the ground-state transition is in this case higher than the one resulting from a direct excitation only. As a consequence, the integrated cross section deduced from this intensity contains a part originating from feeding in addition to the true integrated scattering cross section. Furthermore, a considered level can deexcite not only to the ground state, but also to low-lying excited states (inelastic scattering). In this case, not all observed γ transitions

are ground-state transitions. To deduce the partial width of a ground-state transition Γ_0 and the integrated absorption cross section, one has to know the branching ratio $b_0 = \Gamma_0/\Gamma$. In the present experiment, only a few resolved peaks were observed in the spectrum whereas most of the peaks are expected to form a quasicontinuum because of the huge level density and, consequently, the huge number of transitions in this nuclide. We therefore focus on the determination of the absorption cross section in energy bins applying the formalism just described.

C. Determination of the photoabsorption cross section

In the first step of the analysis, the experimental spectrum was corrected for detector response, for the absolute efficiency and the absolute photon flux, for background radiation, and for atomic processes induced by the impinging photons in the ^{181}Ta target. The detector response was simulated by using the program package GEANT4 [45]. The reliability of the simulation was tested by comparing simulated spectra with measured ones as described in Refs. [23,25,35].

The absolute efficiencies of the HPGe detectors were determined experimentally by using ^{137}Cs and ^{226}Ra calibration sources. The efficiency curves calculated with GEANT4 were adjusted to the absolute experimental values. The absolute photon flux was determined by using the known integrated scattering cross sections of levels in ^{11}B. For interpolation, the photon flux was calculated by using a code [46] based on the approximation given in Ref. [47] and including a screening correction according to Ref. [48]. This flux was corrected for absorption in the Al absorber placed behind the radiator and was then adjusted to the experimental values as is shown in Fig. 2.

To deduce the correct dipole-strength distribution, inelastic transitions have to be removed from the spectrum and the ground-state transitions have to be corrected for their branching ratios b_0. We applied statistical methods to estimate the intensities of branching transitions to low-lying excited levels

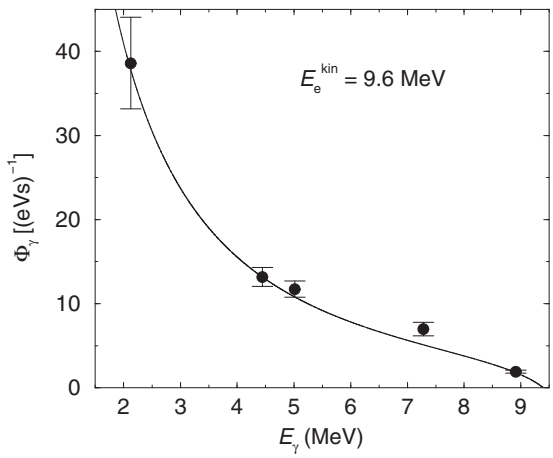

FIG. 2. Absolute photon flux at the target deduced from intensities of five known transitions in ^{11}B (circles) using the efficiency calculated with GEANT4 and the relative flux calculated as described in the text (solid line).

and of the branching ratios of the ground-state transitions. This method was also applied in earlier photon-scattering experiments at ELBE [22–28,33,35,37,49].

At first, a spectrum of the ambient background adjusted to the intensities of the transitions from ^{40}K and ^{208}Tl decay in the in-beam spectrum was subtracted from the measured spectrum. To correct the spectrum for the detector response, spectra of monoenergetic γ rays were calculated in steps of 10 keV by using the simulation code GEANT4. Starting from the high-energy end of the experimental spectrum, the simulated spectra were subtracted sequentially (spectrum-strip method). The background produced by atomic processes in the ^{181}Ta target was obtained from a GEANT4 simulation using the absolute photon flux deduced from the intensities of the transitions in ^{11}B (cf. Fig. 2). The corresponding background spectrum multiplied with the efficiency curve and with the measuring time is also displayed in Fig. 1.

As can be seen in Fig. 1 the spectrum of photons scattered from ^{181}Ta contains only a few resolved peaks but a continuum that is remarkably higher than the background caused by atomic scattering processes. This continuum is formed by a huge number of nonresolved transitions with small intensities which are a consequence of the high nuclear level density at high energy in connection with the finite detector resolution. The relevant intensity of the photons resonantly scattered from ^{181}Ta is obtained from a subtraction of the atomic background from the response-corrected experimental spectrum.

The obtained intensity distribution contains ground-state transitions and, in addition, branching transitions to lower-lying excited states (inelastic transitions) as well as transitions from those states to the ground state (cascade transitions). The different types of transitions cannot be clearly distinguished. However, for the determination of the photoabsorption cross section and the partial widths Γ_0 the intensities of the ground-state transitions are needed. Therefore, contributions of inelastic and cascade transitions have to be subtracted from the spectra. We corrected the intensity distributions by simulating γ-ray cascades [50] from the levels in the whole energy range analogously to the strategy of the Monte Carlo code DICEBOX [51] developed for (n,γ) reactions but including also the excitation from the $7/2^+$ ground state. In these simulations using the code γDEX [22,35,37,49], level schemes (nuclear realizations) including states with $J = 3/2,5/2,\ldots,17/2$ were created. We apply the statistical methods also for the low-energy part of the level scheme instead of using experimentally known low-lying levels in ^{181}Ta, because this would require the knowledge of the partial decay widths of all transitions populating these fixed levels. Fluctuations of the partial widths were treated by applying the Porter-Thomas distribution [52].

Level densities were calculated by using the back-shifted Fermi-gas model with the parameters $a = 18.72(45)$ MeV^{-1} and $E_1 = -0.26(11)$ MeV adjusted to experimental level densities [53]. In the individual nuclear realizations, the values of a and E_1 were varied randomly within their uncertainties. We assumed equal level densities for states with positive and negative parities at the same spin which was proven for odd-mass nuclei in Ref. [54].

The photon strength functions used as the first input for the simulations were assumed to be Lorentz-shaped [55,56]. For the $E1$ strength a combination of two Lorentz functions was used with the parameters $E_0 = 12.30$ MeV, $\sigma_0 = 259$ mb, $\Gamma = 2.43$ MeV, and $E_0 = 15.23$ MeV, $\sigma_0 = 341$ mb, $\Gamma = 4.48$ MeV, respectively, as given in RIPL-3 [57] determined from a fit to the (γ,n) data in Ref. [58]. The maxima were scaled with a factor of 0.85 following the suggestion in Ref. [59]. The parameters for the $M1$ and $E2$ strengths were taken from global parametrizations of $M1$ spin-flip resonances and $E2$ isoscalar resonances, respectively [57].

Spectra of γ-ray cascades were generated for groups of levels in 100 keV bins. Starting from the high-energy end of the experimental spectrum, which contains ground-state transitions only, the simulated intensities of the ground-state transitions were normalized to the experimental ones in the considered bin and the intensity distribution of the branching transitions was subtracted from the experimental spectrum. Applying this procedure step-by-step for each energy bin moving toward the low-energy end of the spectrum one obtains the intensity distribution of the ground-state transitions. Simultaneously, the branching ratios b_0^Δ of the ground-state transitions are deduced for each energy bin Δ. In an individual nuclear realization, the branching ratio b_0^Δ is calculated as the ratio of the sum of the intensities of the ground-state transitions from all levels in Δ to the total intensity of all transitions depopulating those levels to any low-lying levels including the ground state [22–27,33,35,37,49]. To get an impression about the branching ratios, the mean values obtained from the realizations and their uncertainty range are shown in Fig. 3. The mean branching ratio amounts to about 50% for states at 2 MeV and decreases to about 3% at 7 MeV. These percentages are very small compared with the corresponding values for nuclei around mass 90 [23–27] or also for nuclei around mass 140 [33,35] and reflect the huge number of levels and consequently inelastic transitions in this heavy nuclide. By dividing the summed intensities in a bin of the experimental intensity distribution of the ground-state transitions by the corresponding branching ratio we obtain the absorption cross section for a bin as $\sigma_\gamma^\Delta = \sigma_{\gamma\gamma}^\Delta / b_0^\Delta$ in each nuclear realization. Finally, the absorption cross sections of each bin were obtained by averaging over the values of the nuclear realizations. For the uncertainty of the absorption cross section a 1σ deviation from the mean has been taken.

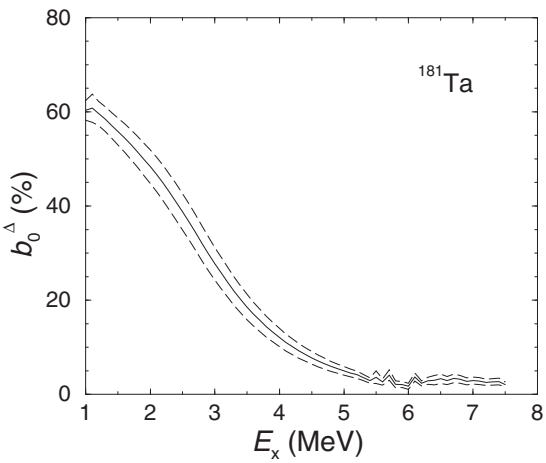

FIG. 3. Mean branching ratios and uncertainty range of ground-state transitions as obtained from the simulations of γ-ray cascades in ^{181}Ta.

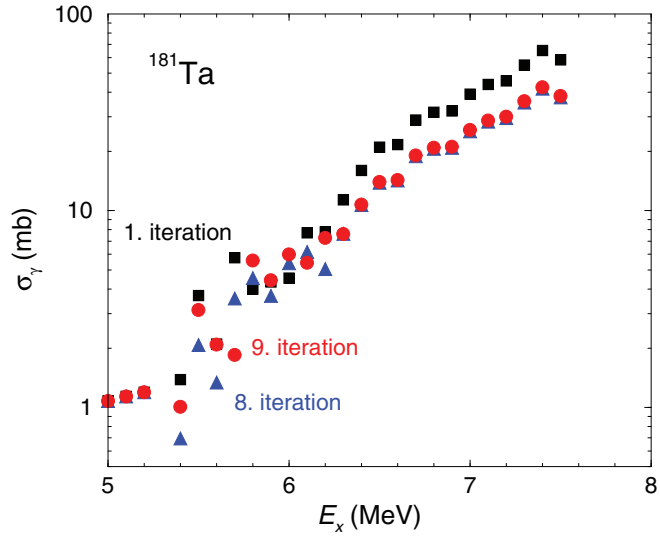

FIG. 4. (Color online) Photoabsorption cross sections obtained from the first (black squares), the eighth (blue triangles), and the ninth (red circles) iterations in the simulation of γ-ray cascades. The iteration was stopped after the ninth step.

The simulations were performed iteratively. The strength function obtained from an iteration step was used as the input for the next step. The iteration was stopped if the input strength function and the output strength function were in agreement within their uncertainties in the energy region above 6.5 MeV. Toward low energy, the uncertainties increase due to the use of the spectrum-strip method and the strength functions do not converge. In Fig. 4 the strength functions obtained from the first, eighth, and ninth iteration step are shown. The iteration was stopped after the ninth step.

The photoabsorption cross section of ^{181}Ta obtained from the present data and the analysis just described is shown in Fig. 5 together with cross sections deduced from (γ,n) experiments [9,58]. The total photoabsorption cross section has been deduced by combining the present (γ,γ') data and the (γ,n) data of Ref. [58]. In Fig. 6 this total cross section is compared with a two-Lorentz curve with the parameters given above. The extension of the GDR to energies below the particle threshold by a Lorentz curve was suggested in Ref. [60]. As can be seen in Fig. 6, the experimental cross section includes considerable extra strength with respect to the approximation of the GDR by a Lorentz curve in the energy range from about 6 to 8 MeV. In the following sections we compare the experimental ^{181}Ta dipole strength with results of calculations obtained within the framework of the quasiparticle-random-phase approximation (QRPA) in a deformed potential, and calculate reaction rates using the statistical model code TALYS having implemented our photoabsorption cross section as an input.

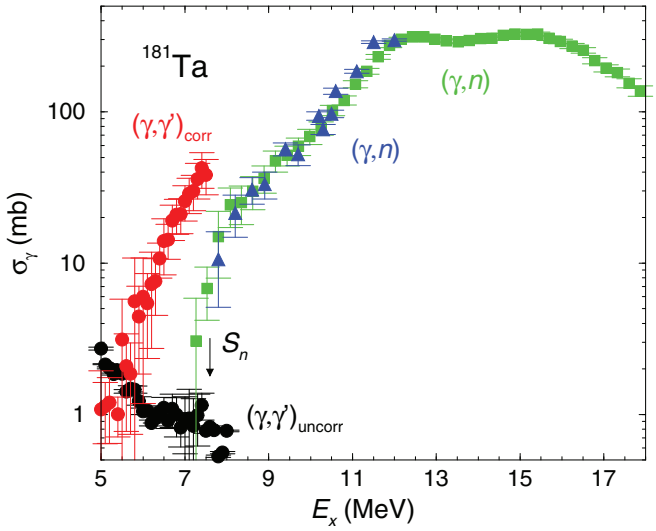

FIG. 5. (Color online) Photoabsorption cross sections before (black circles) and after (red circles) correction for inelastic transitions and branching ratios in comparison with (γ,n) data from Ref. [58] (green squares) and Refs. [9,10] (blue triangles).

III. QRPA CALCULATIONS

For the calculation of the absorption cross section of ^{181}Ta we use the quasiparticle-random-phase approximation (QRPA), explained in detail in Ref. [61], with the Hamiltonian

$$H_{E1}^{\mathrm{QRPA}} = h_{\mathrm{MF}} - \frac{1}{2}\sum_{t=0,1}\sum_{\mu=-1,+1}\kappa_{1\mu}^{t} Q_{1\mu}^{t} Q_{1-\mu}^{t} - \frac{1}{2}\sum_{t=0,1}\sum_{\mu=-3,+3}\kappa_{3\mu}^{t} Q_{3\mu}^{t} Q_{3-\mu}^{t}. \quad (3)$$

Here, h_{MF} stands for the quasiparticle Hamiltonian. It consists of a Woods-Saxon mean field and a monopole pair potential. The isoscalar ($t = 0$) and isovector ($t = 1$) parts of the dipole ($\lambda = 1$) and octupole ($\lambda = 3$) interaction are included by defining the multipole operators $Q_{\lambda\mu}^{t} = [r^{\lambda}Y_{\lambda\mu}]^{\pi} + (-1)^{t}[r^{\lambda}Y_{\lambda\mu}]^{\nu}$. The values $\kappa_{\lambda\mu}^{t=1}$ were adjusted such that they reproduce the average energy of the maxima of the GDR. The suppression of the spurious center-of-mass motion [62] allows us to calculate transition strengths. It is not necessary to assume an effective charge for the neutrons, so the bare proton charge e_{π} can be used. The transition operator is then given by

$$\hat{M}(E1)_{\mu} = e_{\pi}\sum_{i=1}^{Z}[rY_{1\mu}]_{i}. \quad (4)$$

The calculations were carried out with a quadrupole deformation of $\beta_2 = 0.25$. The resulting QRPA spectrum is shown in Fig. 6. The QRPA solutions were folded with Lorentz functions of 250 keV width, which still produces the usual fluctuations of the QRPA cross section. A smooth curve is obtained when applying a greater smearing width of 3 MeV. In each case, there is strength missing at low energy and in particular in the region of enhanced strength found between 6 and 8 MeV.

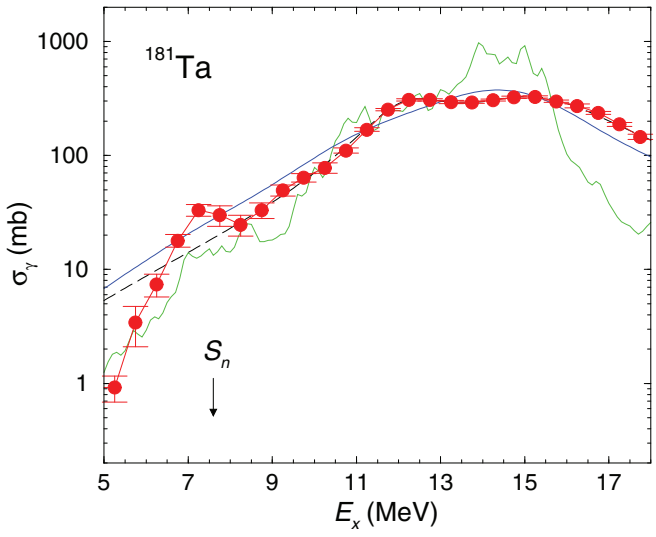

FIG. 6. (Color online) Total photoabsorption cross section of ^{181}Ta obtained by combining the present (γ,γ') data and the (γ,n) data of Ref. [58]. The data were averaged over 0.5 MeV bins to reduce statistical fluctuations. The black dashed line represents a double-Lorentz distribution with the parameters given in the text. The jagged green and smooth blue solid lines are the results of the QRPA calculations discussed in Sec. III, folded with Lorentz curves of smearing widths of 0.25 and 3.0 MeV, respectively.

IV. CALCULATIONS OF CROSS SECTIONS USING EXPERIMENTAL STRENGTH FUNCTIONS

To investigate the impact of using an experimental γ-ray strength function, rather than standard parametrizations, we have performed (n,γ) and (γ,n) cross-section calculations using the nuclear reaction computer code TALYS (version 1.2) [41]. The standard strength functions implemented in TALYS are the single Lorentz curve (SLO) [55,56] and the generalized Lorentz curve (GLO) [63,64]. In both the SLO and the GLO approach the GSF is parametrized in terms of the width, energy, and cross section of the GDR, whereas nuclear deformation is not explicitly accounted for. A double-Lorentz curve (DLO), which takes into account the axial-symmetric nuclear deformation, is used in the popular computer code NON-SMOKER [65]. The DLO model also describes the strength function in terms of GDR parameters, and is composed of two Lorentzian dipole vibrations: one along and one perpendicular to the axis of rotation. In this context, we also mention that an extension to triaxial shapes (TLO) was recently proposed. The TLO description is composed of three Lorentzians and uses global parameters for the centroids and widths of the three curves [66]. The experimental photoabsorption cross section (EPACS) and the related strength function are a combination of the present (γ,γ') data and the (γ,n) data discussed in Sec. II C. For the calculations presented here, the GLO, SLO, DLO,

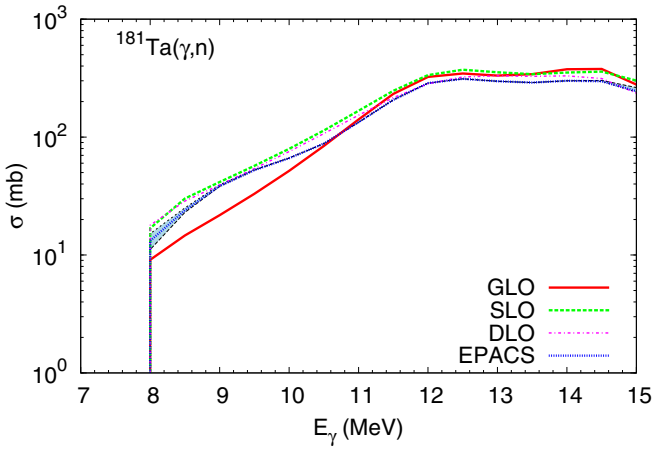

FIG. 7. (Color online) ^{181}Ta(γ,n) cross sections as functions of γ-ray energy calculated using the code TALYS with various models for the input strength function. The uncertainty of the EPACS shown as a blue (gray) band results from the use of various nuclear level-density models (see text).

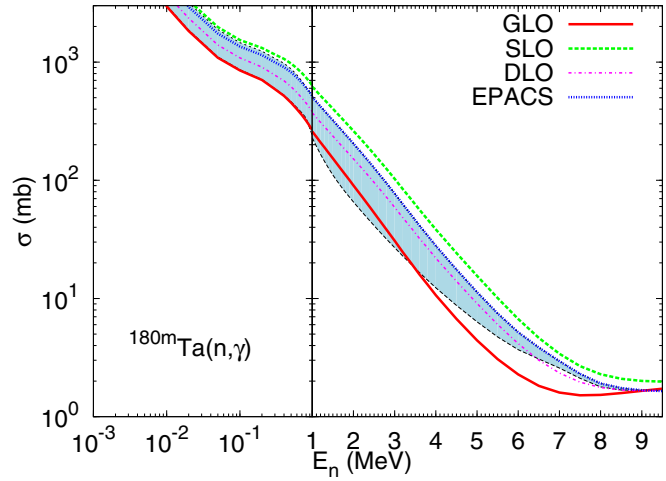

FIG. 9. (Color online) Same as Fig. 8, but for ^{180m}Ta(n,γ) cross sections.

and EPACS strength functions have been combined with the constant-temperature level density model [67]. Further details of this procedure and of the TALYS calculations are given in Ref. [68].

The calculated ^{181}Ta(γ,n), ^{180}Ta(n,γ), and ^{180m}Ta(n,γ) cross sections are shown in Figs. 7, 8, and 9, respectively. Figures 8 and 9 show that enhancement in the strength function over an energy region below 7 MeV gives rise to a slightly increased (n,γ) cross section. To evaluate the uncertainty of the EPACS originating from the nuclear level density (NLD) model, we repeated the cross-section calculations using a variety of NLD models available in the TALYS package. While microscopic level density models based on the Hartree-Fock calculation [69] underestimate the experimental data, the constant-temperature level density model, back-shifted Fermi-gas model [70], generalized superfluid model [71,72], and combinatorial model [73] can well reproduce the experimental data (see also Fig. 5). The estimated uncertainties for the EPACS are shown as a light-blue (gray) belt in the figures.

The comparison with the direct measurement of ^{180m}Ta(n,γ) Maxwellian-averaged cross sections (MACS) of KADoNiS (version 0.2) [68] in the energy from 10 to 120 keV, which is related to the s-process energy region, is shown in Fig. 10. The EPACS results clearly exceed the result of KADoNiS. On the other hand, the results of SLO has a tendency similar to EPACS but are even greater. GLO and DLO are lower than the result of EPACS but included within the uncertainty of EPACS. The effects of the additional strength in EPACS is averaged out over the entire cross section due to the γ cascade. Because the structural features in the

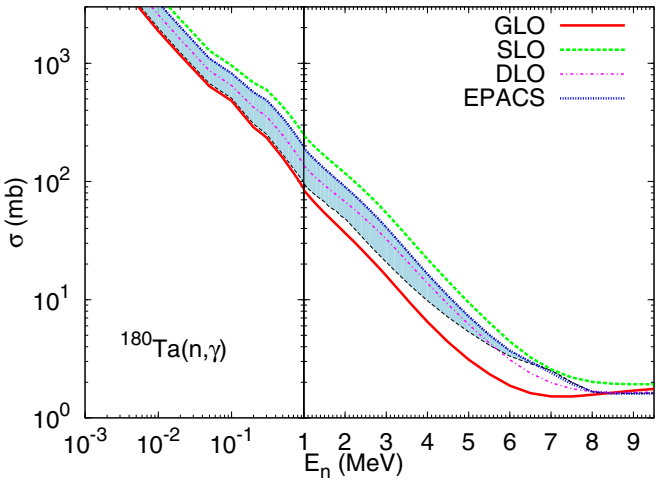

FIG. 8. (Color online) ^{180}Ta(n,γ) cross sections as functions of neutron energy calculated using the code TALYS with various models for the input strength function. The uncertainty of the EPACS shown as a blue (gray) band results from the use of various nuclear level density models.

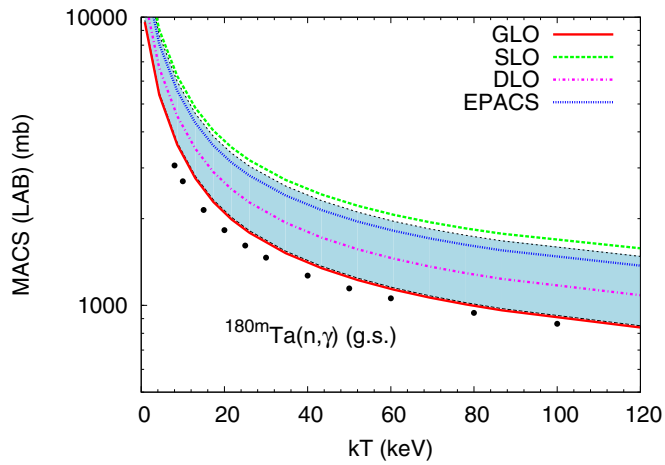

FIG. 10. (Color online) ^{180m}Ta(n,γ) Maxwellian-averaged cross sections calculated using the code TALYS with various models for the input strength function compared with KADoNiS (version 0.2) (black circles). The uncertainty of the EPACS shown as a blue (gray) band results from the use of various nuclear level density models.

strength function are below the neutron-separation energy ($S_n = 7.58$ MeV), they are not visible in the (γ,n) channel.

V. STELLAR REACTION RATES

In stellar environments nuclei occupy not only their ground states but also a spectrum of thermally enhanced excited states. As such, calculations of reaction rates have to include these excited contributions. In TALYS the stellar photodissociation rates are calculated as a function of temperature T from the expression

$$\lambda^{*}_{(\gamma,j)}(T) = \frac{\sum_{\mu}(2J^{\mu}+1)\lambda^{\mu}_{(\gamma,j)}(T)\exp\left(-\epsilon^{\mu}_{x}/k_{B}T\right)}{\sum_{\mu}(2J^{\mu}+1)\exp\left(-\epsilon^{\mu}_{x}/k_{B}T\right)}, \quad (5)$$

where J^{μ} is the spin of the target nucleus in thermally populated state μ, with excitation energy ϵ_x. The photodissociation rates $\lambda^{\mu}_{(\gamma,j)}(T)$ for individual states can be determined from

$$\lambda^{\mu}_{(\gamma,j)}(T) = \int_{0}^{\infty} c\,\sigma^{\mu}_{(\gamma,j)}(E) n_{\gamma}(E,T)\,dE, \quad (6)$$

where c is the speed of light, $\sigma^{\mu}_{(\gamma,j)}(E)$ is the photodissociation cross section, and $n(E_{\gamma},T)$ is the black-body γ-ray spectrum which describes the energy distribution of photons in the stellar environment. Similarly, (n,γ) rates are calculated by integrating $\sigma^{\mu}_{(j,\gamma)}(E)$ [i.e., the (n,γ) cross sections] with a Maxwell-Boltzmann distribution for the neutrons.

We have used TALYS to investigate the impact of the experimentally determined γ-ray strength functions on the ^{181}Ta(γ,n), ^{180m}Ta(n,γ), and ^{180}Ta(n,γ) reaction rates. Displayed in Figs. 11, 12, and 13, respectively, are the ^{181}Ta(γ,n), ^{180}Ta(n,γ), and ^{180m}Ta(n,γ) reaction rates calculated using EPACS, compared to identical calculations using the SLO and GLO strength functions. For the (n,γ) rate, the calculation is also compared to the DLO strength function. Figure 11 shows that the commonly used phenomenological models predict

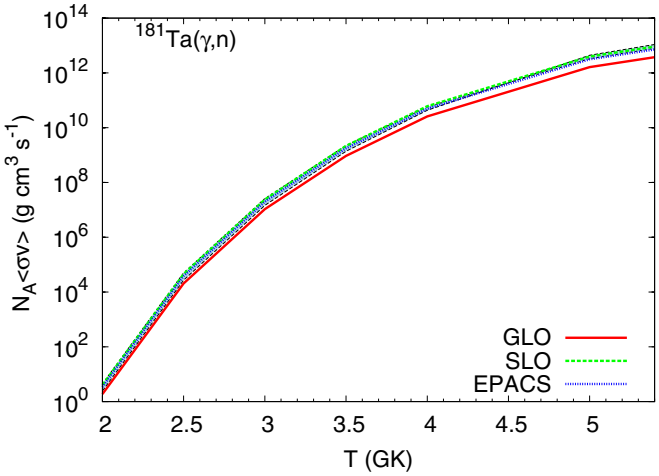

FIG. 11. (Color online) ^{181}Ta(γ,n) reaction rates as a function of temperature, calculated using the code TALYS with various models for the input strength function. The uncertainty of the EPACS shown as a blue band results from the use of various nuclear level density models.

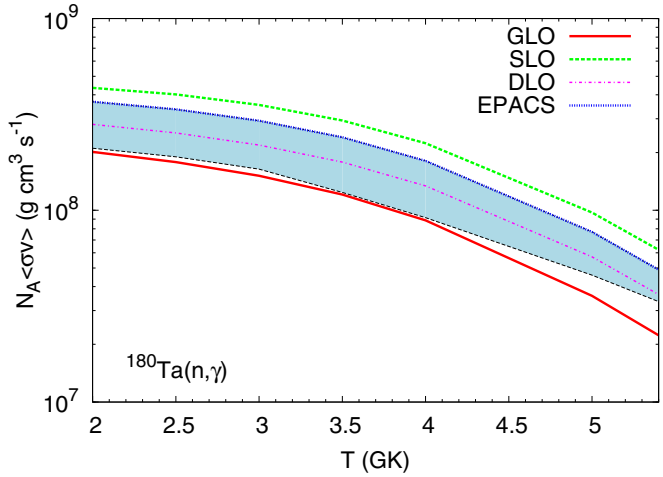

FIG. 12. (Color online) Same as Fig. 11, but for ^{180}Ta(n,γ) reaction rates.

(γ,n) reaction rates which are in very good agreement with the rate obtained using the measured strength function.

Figure 13 shows the comparison with the KADoNiS reaction rate of ^{180m}Ta(n,γ). The calculated result using TALYS including EPACS overestimates the result of KADoNiS. A possible explanation for this is uncertainty of the stellar enhancement factor for both TALYS calculations and KADoNiS. However, our result and the direct measurement of the neutron capture cross section for ^{180m}Ta still show some discrepancy.

VI. CONCLUSION

The dipole-strength distribution in ^{181}Ta up to the neutron-separation energy has been studied in a photon-scattering experiment at the ELBE accelerator using an kinetic electron energy of 9.6 MeV. The intensity distribution obtained from the measured spectra after a correction for detector response

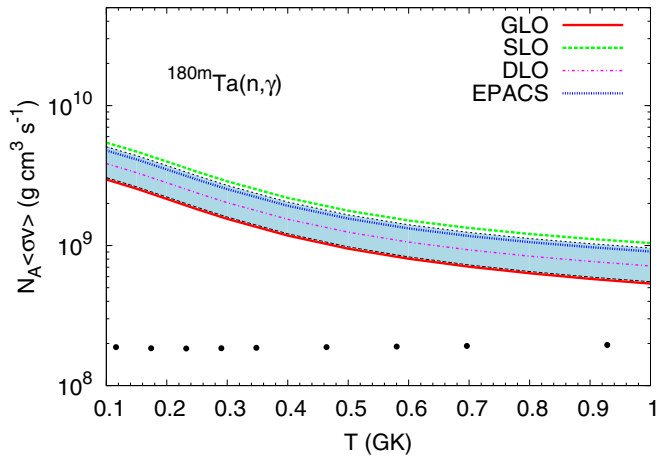

FIG. 13. (Color online) ^{180m}Ta(n,γ) reaction rates as a function of temperature, calculated using the code TALYS with various models for the input strength function compared with KADoNiS (version 0.2) (black circles). The uncertainty of the EPACS shown as a blue(gray) band results from the use of various nuclear level density models.

and a subtraction of background radiation produced by interaction of the γ rays with the target atoms contains a dominating quasicontinuum from which the scattering cross section for energy bins was deduced. For the determination of the absorption cross section, simulations of statistical γ-ray cascades were performed to estimate the intensities of inelastic transitions and the branching ratios of the ground-state transitions. The photoabsorption cross section obtained from this procedure connects continuously to (γ,n) data and gives new information about the extension of the dipole-strength distribution toward energies around and below the threshold of the (γ,n) reaction. In comparison with a straightforward approximation of the GDR by a Lorentz curve we observe extra $E1$ strength in the energy range from 6 to 8 MeV. This extra $E1$ strength may be considered as a pygmy dipole resonance. By using the experimentally determined γ-ray strength function for ^{181}Ta, the stellar neutron capture rates for ^{180}Ta and ^{180m}Ta were evaluated. The evaluated ^{180}Ta and ^{180m}Ta stellar neutron capture rates are also enhanced by extra $E1$ strength. However, our present result and the direct measurement of the neutron capture cross section for ^{180m}Ta still show some discrepancy.

ACKNOWLEDGMENTS

We thank the staff of the ELBE accelerator for their cooperation during the experiments and A. Hartmann for technical assistance. We also thank Prof. H. Utsunomiya for his teaching in the early stage of this work and in the photoneutron experiment. A.M. thanks Prof. K. Kato (Hokkaido University), Dr. N. Otsuka (IAEA), and Dr. T. Hayakawa and Dr. T. Shizuma (JAEA) for their advice on this work. A.M. was supported by Helmholtz-Zentrum Dresden-Rossendorf, by IAEA, and by Hokkaido University. R.M. was supported by Deutsche Forschungsgemeinschaft under Project No. SCHW 883/1-1.

[1] G. A. Bartholomew, E. D. Earle, A. J. Ferguson, J. W. Knowles, and M. A. Lone, Adv. Nucl. Phys. **7**, 229 (1973).
[2] A. Makinaga *et al.*, Phys. Rev. C **79**, 025801 (2009).
[3] H. Utsunomiya *et al.*, Phys. Rev. C **81**, 035801 (2010).
[4] M. Arnould and S. Goriely, Phys. Rep. **384**, 1 (2003).
[5] K. Wisshak, F. Voss, C. Arlandini, F. Käppeler, M. Heil, R. Reifarth, M. Krtička, and F. Bečvář, Phys. Rev. C **69**, 055801 (2004).
[6] H. Beer and R. A. Ward, Nature (London) **291**, 308 (1981).
[7] K. Yokoi and K. Takahashi, Nature (London) **305**, 198 (1983).
[8] S. E. Woosley, D. H. Hartmann, R. D. Hoffmann, and W. C. Haxton, Astrophys. J. **356**, 272 (1990).
[9] H. Utsunomiya *et al.*, Phys. Rev. C **67**, 015807 (2003).
[10] S. Goko *et al.*, Phys. Rev. Lett. **96**, 192501 (2006).
[11] D. Belic *et al.*, Phys. Rev. C **65**, 035801 (2002).
[12] F. Käppeler, C. Arlandini, M. Heil, F. Voss, and K. Wisshak, R. Reifarth, O. Straniero, R. Gallino, S. Masera, and C. Travaglio, Phys. Rev. C **69**, 055802 (2004).
[13] P. Mohr, F. Käppeler, and R. Gallino, Phys. Rev. C **75**, 012802(R) (2007).
[14] T. Hayakawa, T. Kajino, S. Chiba, and G. J. Mathews, Phys. Rev. C **81**, 052801(R) (2010).
[15] A. Heger, E. Kolbe, W. C. Haxton, K. Langanke, G. Martínez-Pinedo, and S. E. Woosley, Phys. Lett. B **606**, 258 (2005).
[16] A. Byelikov *et al.*, Phys. Rev. Lett. **98**, 082501 (2007).
[17] E. Anders and N. Grevesse, Geochim. Cosmochim. Acta **53**, 197 (1989).
[18] Myung-Ki Cheoun, Eunja Ha, T. Hayakawa, Toshitaka Kajino, and Satoshi Chiba, Phys. Rev. C **82**, 035504 (2010).
[19] K. Takahashi and K. Yokoi, At. Data Nucl. Data Tables **36**, 375 (1987).
[20] A. Wolpert *et al.*, Phys. Rev. C **58**, 765 (1998).
[21] P. M. Goddard *et al.*, Phys. Rev. C **88**, 064308 (2013).
[22] G. Schramm *et al.*, Phys. Rev. C **85**, 014311 (2012).
[23] G. Rusev *et al.*, Phys. Rev. C **77**, 064321 (2008).
[24] G. Rusev *et al.*, Phys. Rev. C **79**, 061302(R) (2009).
[25] R. Schwengner *et al.*, Phys. Rev. C **76**, 034321 (2007).
[26] R. Schwengner *et al.*, Phys. Rev. C **78**, 064314 (2008).
[27] N. Benouaret *et al.*, Phys. Rev. C **79**, 014303 (2009).
[28] R. Schwengner *et al.*, Phys. Rev. C **87**, 024306 (2013).
[29] A. Zilges, S. Volz, M. Babilon, T. Hartmann, P. Mohr, and K. Vogt, Phys. Lett. B **542**, 43 (2002).
[30] P. Adrich *et al.*, Phys. Rev. Lett. **95**, 132501 (2005).
[31] S. Volz, N. Tsoneva, M. Babilon, M. Elvers, J. Hasper, R.-D. Herzberg, H. Lenske, K. Lindenberg, D. Savran, and A. Zilges, Nucl. Phys. A **779**, 1 (2006).
[32] D. Savran, M. Fritzsche, J. Hasper, K. Lindenberg, S. Müller, V. Yu. Ponomarev, K. Sonnabend, and A. Zilges, Phys. Rev. Lett. **100**, 232501 (2008).
[33] A. Makinaga *et al.*, Phys. Rev. C **82**, 024314 (2010).
[34] A. P. Tonchev, S. L. Hammond, J. H. Kelley, E. Kwan, H. Lenske, G. Rusev, W. Tornow, and N. Tsoneva, Phys. Rev. Lett. **104**, 072501 (2010).
[35] R. Massarczyk *et al.*, Phys. Rev. C **86**, 014319 (2012).
[36] J. Isaak *et al.*, Phys. Lett. B **727**, 361 (2013).
[37] R. Massarczyk *et al.*, Phys. Rev. C **87**, 044306 (2013).
[38] N. Ryezayeva, T. Hartmann, Y. Kalmykov, H. Lenske, P. von Neumann-Cosel, V. Y. Ponomarev, A. Richter, A. Shevchenko, S. Volz, and J. Wambach, Phys. Rev. Lett. **89**, 272502 (2002).
[39] T. Shizuma, T. Hayakawa, H. Ohgaki, H. Toyokawa, T. Komatsubara, N. Kikuzawa, A. Tamii, and H. Nakada, Phys. Rev. C **78**, 061303(R) (2008).
[40] R. Schwengner *et al.*, Phys. Rev. C **81**, 054315 (2010).
[41] A. J. Koning, S. Hilaire, and M. C. Duijvestijn, AIP Conf. Proc. **769**, 1154 (2005).
[42] R. Schwengner *et al.*, Nucl. Instr. Meth. A **555**, 211 (2005).
[43] F. Ajzenberg-Selove, Nucl. Phys. A **506**, 1 (1990).
[44] G. Rusev, A. P. Tonchev, R. Schwengner, C. Sun, W. Tornow, and Y. K. Wu, Phys. Rev. C **79**, 047601 (2009).
[45] S. Agostinelli *et al.*, Nucl. Instr. Meth. A **506**, 250 (2003).
[46] E. Haug, Rad. Phys. Chem. **77**, 207 (2008).
[47] G. Roche, C. Ducos, and J. Proriol, Phys. Rev. A **5**, 2403 (1972).
[48] F. Salvat, J. D. Martinez, R. Mayol, and J. Parellada, Phys. Rev. A **36**, 467 (1987).

[49] R. Massarczyk *et al.*, Phys. Rev. Lett. **112**, 072501 (2014).
[50] G. Rusev, Dissertation, Technische Universität Dresden, 2007, Report FZD-478 (ISSN 1437-322X), http://fzd.de/publications/010008/10008.pdf.
[51] F. Bečvář, Nucl. Instrum. Methods A **417**, 434 (1998).
[52] C. E. Porter and R. G. Thomas, Phys. Rev. **104**, 483 (1956).
[53] T. von Egidy and D. Bucurescu, Phys. Rev. C **80**, 054310 (2009).
[54] S. I. Al-Quraishi, S. M. Grimes, T. N. Massey, and D. A. Resler, Phys. Rev. C **67**, 015803 (2003).
[55] D. M. Brink, Nucl. Phys. **4**, 215 (1957).
[56] P. Axel, Phys. Rev. **126**, 671 (1962).
[57] R. Capote *et al.*, Nucl. Data Sheets **110**, 3107 (2009).
[58] R. Bergere, H. Beil, and A. Veyssiere, Nucl. Phys. A **121**, 463 (1968).
[59] B. L. Berman, R. E. Pywell, S. S. Dietrich, M. N. Thompson, K. G. McNeill, and J. W. Jury, Phys. Rev. C **36**, 1286 (1987).
[60] C. B. Dover, R. H. Lemmer, and F. J. W. Hahne, Ann. Phys. (NY) **70**, 458 (1972).
[61] F. Dönau, G. Rusev, R. Schwengner, A. R. Junghans, K. D. Schilling, and A. Wagner, Phys. Rev. C **76**, 014317 (2007).
[62] F. Dönau, Phys. Rev. Lett. **94**, 092503 (2005).
[63] S. G. Kadmensky, V. P. Markushev, and V. I. Furman, Sov. J. Nucl. Phys. **37**, 165 (1983).
[64] J. Kopecky and M. Uhl, Phys. Rev. C **41**, 1941 (1990).
[65] T. Rauscher and F.-K. Thielemann, in *Stellar Evolution, Stellar Explosions and Galactic Chemical Evolution*, edited by A. Mezzacappa (IOP, Bristol, 1998), p. 519.
[66] A. R. Junghans, G. Rusev, R. Schwengner, A. Wagner, and E. Grosse, Phys. Lett. B **670**, 200 (2008).
[67] A. Gilbert and A. G. W. Cameron, Can. J. Phys. **43**, 1446 (1965).
[68] M. Beard, S. Frauendorf, B. Kämpfer, R. Schwengner, and M. Wiescher, Phys. Rev. C **85**, 065808 (2012).
[69] S. Goriely, F. Tordeur, and J. M. Pearson, Atom. Data Nucl. Data Tables **77**, 311 (2001).
[70] W. Dilg, W. Schantl, H. Vonach, and M. Uhl, Nucl. Phys. A **217**, 269 (1973).
[71] A. V. Ignatyuk, K. K. Istekov, and G. N. Smirenkin, Sov. J. Nucl. Phys. **29**, 450 (1979).
[72] A. V. Ignatyuk, J. L. Weil, S. Raman, and S. Kahane, Phys. Rev. C **47**, 1504 (1993).
[73] S. Goriely, S. Hilaire, and A. J. Koning, Phys. Rev. C **78**, 064307 (2008).